JMEPEG (2012) 21:1553–1561
DOI: 10.1007/s11665-011-0063-5

1059-9495/$19.00

Simulation of Static Recrystallization After Cold Side-Pressing of Low Carbon Steels Using Cellular Automata

E. Afshari and S. Serajzadeh

(Submitted June 7, 2011)

In this article, the finite element and cellular automata models are coupled to determine static recrystallization kinetics after cold deformation of low carbon steels. The deformation analysis is first performed to predict the strain, stress, and stored energy distributions within the deformed steel employing the finite element software, ABAQUS. Then, the kinetics of static recrystallization and distribution of recrystallized grain size are evaluated by means of a cellular automata model together with the stored energy calculated by the deformation analysis. To examine the predictions, the experimental results of recrystallized fractions and grain sizes after cold side-pressing of low carbon steel are compared with the predicted ones, and a reasonable agreement is achieved.

Keywords cellular automata, cold deformation, finite element analysis, static recrystallization

1. Introduction

As a general rule, cold plastic deformation leads to the increase of dislocation density as well as stored energy within the deformed metal, while it serves as a driving force for the subsequent recrystallization associating with nucleation and growth processes (Ref 1, 2). As a result, recrystallization can strongly affect the microstructures of deformed material and the final mechanical properties. In this regard, prediction of recrystallization behavior is of importance to understand the effects of process parameters on final microstructures within the industrial parts (Ref 3, 4). Among the various modeling approaches, cellular automata technique (CA) is considered an applicable and powerful route to assess microstructural changes during static recrystallization. In this method, the system is divided into cells characterized by state variables that are transformed according to specific rules which play the role of governing equations and more effectively express local conditions and structural details than those do the usual continuum models. Recently, CA methods have been employed in modeling static recrystallization (Ref 5-16) as well as dynamic recrystallization (Ref 17-22) mainly assuming uniform distribution of stored energy within the material as well as taking arbitrarily nucleation models in recrystallization simulation.

Note that in a proper recrystallization modeling, it is vital to know both annealing conditions and the distribution of strain field from pervious metal processing**.** Therefore, integrated model which incorporates the deformation modeling with probabilistic laws such CA models in recrystallization simulation provides a powerful tool to consider the initial strain field on recrystallization kinetics (Ref 4). Therefore, in this study, finite element analysis and cellular automata model have been coupled to accurately determine the kinetics of static recrystallization as well as the grain size distribution after recrystallization of cold deformed steel. In order to examine accuracy of modeling result, experimental testing has also been carried out. First, compressing of cylindrical samples from lateral surface, known as side pressing has been performed under different reductions then, the deformed samples have been annealed isothermally in different temperatures and time intervals. Finally, the hardness values have been measured to determine recrystallized fraction. The metallographic examination has also been performed on the cross section of recrystallized specimens to evaluate grain size distribution after static recrystallization.

E. Afshari and **S. Serajzadeh**, Department of Materials Science and Engineering, Sharif University of Technology, Azadi Avenue, Tehran, Iran. Contact e-mails: e_afshari@mehr.sharif.edu and serajzadeh@sharif.edu.

2. Mathematical Modeling

In this study, a mathematical model is first used to predict stress and strain fields and the distribution of stored energy within the cold deformed metal employing the finite element software, ABAQUS/Explicit. The calculated stored energy from the analysis is then utilized in the cellular automata model to determine static recrystallization kinetics as well as to evaluate the distribution of grain size. Accordingly, the process of side-pressing of low carbon steel is considered in the deformation model in which dies are taken as rigid bodies and the sample is taken as an elastic-plastic material. According to the geometry of deformation and sample dimensions, i.e., diameter of 15 mm and length of 40 mm, plane strain condition is assumed in the deformation model. Thus, a plane strain elastic-plastic finite element model is employed in the *x-y* plane of cylindrical specimen as the deformation domain where 1600 rectangular eight-node elements are used as shown in Fig. 1. In addition, the bottom die is constrained in all the directions, and the top die movement was limited in y-direction, and a constant

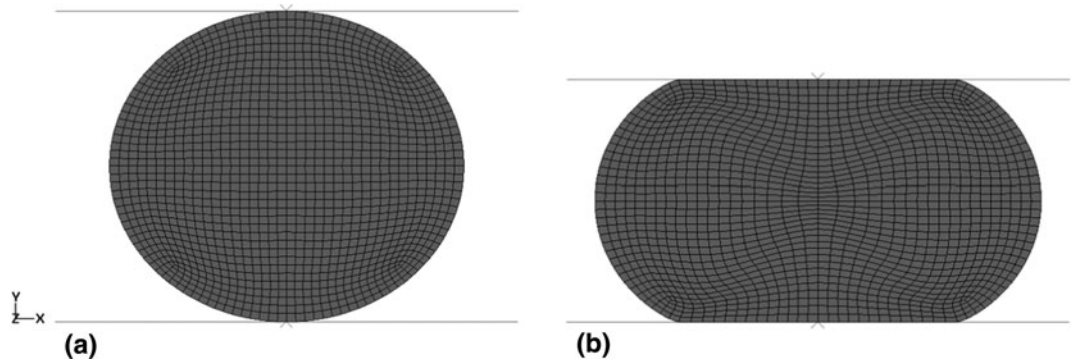

Fig. 1 The mesh system in the deformation model: (a) before cold deformation and (b) after side-pressing with reduction of 25%

friction factor of 0.09 is taken at the contact region between the die and the deforming metal.

In the next stage, recrystallization kinetics in different regions of side-pressed steel, each of which having an area of 0.64 mm^2, are modeled using a two-dimensional CA consisting of 40000 square cells with the dimensions of 4 μm × 4 μm. The state of each cell is defined using three rules: (1) orientation variable with defining an integer number to each cell representing its crystallographic orientation, (2) energy variable, and (3) sort variable determining whether the cell belongs to the deformed state, recrystallized state, or the interface.

In the CA model, a matrix is first generated for describing the initial grain size distribution including different crystallographic orientations and the stored energy distribution achieved from the deformation analysis. In the second step, cells with higher stored energy act as nucleation site according to a probability related to the level of stored energy within each cell. In the last step, recrystallized nuclei begin to grow into the non-recrystallized neighbors using a probabilistic transformation rule.

Note that the nucleation mechanism is defined based on the assumption of site-saturated nucleation, and it should be mentioned that nucleation and growth probability laws are employed while the simulated microstructures should be consistent with the experimental values. In this regard, the mean grain size is calculated as below (Ref 11):

$$D = \sqrt{\frac{kL_{CA}^2}{N}} \quad \text{(Eq 1)}$$

here L_{CA} is the size of a single cell, k represents the number of cells in the employed lattice, and N denotes total number of the grains. As noted above, since CA model is not basically calibrated by any physical length of time scale (Ref 4), the appropriate L_{CA} is determined by comparing average grain size in simulated microstructure with the real ones achieved from the test samples.

The distribution of stored energy is also required in recrystallization modeling to assess a proper nucleation rate as well as to accurately predict grain boundary mobility. Therefore, dislocation density may be estimated using the predicted stress field by the finite element modeling and the following equation (Ref 1):

$$\rho_i = \sqrt{\frac{\sigma_i}{\alpha G b}} \quad \text{(Eq 2)}$$

here ρ_i is the dislocation density of σ_i the flow stress of the same point, G is the shear modulus, b is the burgers vector, and α is a material constant usually taken as 0.5 (Ref 2). Finally, the stored energy in each point may be calculated as follows (Ref 1, 12):

$$E_D = \alpha \rho_i G b^2 \quad \text{(Eq 3)}$$

In order to map the stored energy distribution of the cold-deformed sample to the CA lattice, the cross section of the sample is first divided into several regions according to the predicted stress field at the end of deformation operation, and then a mean value of stored energy is allocated to each region using Eq 2 and 3. In fact, it is assumed that the inhomogeneously deformed metal consists of homogeneously deformed sub-regions.

Heterogeneous nucleation may occur during recrystallization in which some points with high local stored energy become preferred sites for nucleation (Ref 1). Considering the nucleation rate as a thermally activated phenomenon as well as affected by the level of stored energy, the following equation may be employed to describe nucleation rate (Ref 22):

$$\dot{N} = C_0 (E_D + E_B - E_C) \exp\left(\frac{-Q_a}{RT}\right) \quad \text{(Eq 4)}$$

where E_D is the stored energy owing to dislocation density, E_B is the grain boundary energy, E_C is the critical energy for initiating new grain (Ref 23). Q_a denotes the nucleation activation energy, R is the gas constant, T is temperature, and C_0 is a constant. The grain boundary energy can be calculated using the Read-Shockley (Ref 1, 20) equation as:

$$\gamma = \gamma_m \frac{\theta_i}{\theta_m}\left(1 - \ln\frac{\theta_i}{\theta_m}\right) \quad \text{(Eq 5)}$$

$$E_B = \frac{3\gamma}{D} \quad \text{(Eq 6)}$$

here θ_i is the grain boundary misorientation between the ith recrystallized grain and its neighboring grain, θ_m is the misorientation of high angle grain boundary which is usually taken as 15° (Ref 1), γ_m is the grain boundary energy for $\theta_i > \theta_m$, and D is the grain diameter. Besides, it should be noted that the effect of static recovery on the stored energy is ignored due to its slow kinetics in low carbon steels (Ref 24).

After nucleation stage, the stable nuclei start to grow and the difference of the stored energy between the deformed and the recrystallized regions provides the driving force for continuing recrystallization process. Also, the velocity of recrystallized boundary "V" may be expressed by the following equation:

$$V = MP \quad \text{(Eq 7)}$$

where P is the driving pressure for the recrystallization which is function of stored energy within the deformed matrix. M represents the grain boundary mobility that may be calculated as follows (Ref 22):

$$M = \frac{D_0 b^2}{KT} \exp\left(\frac{-Q_b}{RT}\right) \quad \text{(Eq 8)}$$

here D_0 is the coefficient of boundary self-diffusion, b is Burgers vector, K is Boltzman constant, and Q_b is the grain boundary activation energy. In the growth step according to the CA rule, the states of all recrystallized cells are remained unchanged and an unrecrystallized cell stayed untouched unless there is a recrystallized cell in its neighborhood. If so, it could become part of the growing grain with probability, w_g which can be calculated as below (Ref 3):

$$w_g^{\text{local}} = \left(\frac{wP^{\text{local}} M^{\text{local}}}{wP^{\max} M^{\max}}\right) \quad \text{(Eq 9)}$$

It is assumed that the velocity of grain boundary is proportional to the pressure (Ref 1) and also, a parameter, i.e., "Z," is introduced to express the pining effect as follows:

$$V = ZMP \quad \text{(Eq 10)}$$

here "Z" is a constant which is taken as 0.7 in this study. This factor was determined based on a trial analysis carried out through on a series of test samples. The samples were deformed in uni-axial tensile testing machine to ensure homogenous deformation under two elongations of 16 and 25%. Then, the CA model was conducted on these samples with different pinning factor ranging between 0.5 and 1. Finally, the output of the model was compared with experimental data, i.e., mean grain size as indicated in Eq 1, and the value of 0.7 was observed to reasonably match the experimental observations. It should be noted that through this analysis the appropriate CA cell, $L_{CA,}$ size was also determined. In fact, an optimization program based on the mean sum square error was developed to evaluate proper values of L_{CA} and Z-factor at the same time for the employed steel.

In order to verify the achieved grain size and recrystallization kinetic, it is necessary to convert CA steps into real time. The time step of the simulation is calculated using amount of stored energy and length scale of cell, L_{CA} from Eq 8 and 10 as

$$\Delta t = \frac{KTL_{CA}}{ZD_0 b^2 P \exp\left(\frac{-Q_b}{RT}\right)} \quad \text{(Eq 11)}$$

As mentioned before, simulation is carried out on low carbon steel, while the corresponding parameters are listed in Table 1.

Table 1 The parameters used in the present model

D_0, m^2/s	b, m	G, N/m^2	γ, J/m^2	Q_a, kJ/mol	Q_b, kJ/mol
1.1×10^6	2.5×10^{-10}	8×10^{10}	0.6	170	140

3. Experimental Procedures

The experimental studies were carried out on low carbon steel rod with chemical composition listed in Table 2 where the initial mean grain size was about 130 μm. Tensile testing was conducted according to ASTM E8M on the steel rod to obtain nominal stress-strain relationship. Figure 2 shows the nominal stress-strain behavior of the steel. Note that these data were first converted to real stress-strain values as a tabulated data and then were implemented in the model for describing the flow stress behavior of the steel. Cylindrical specimens of 15-mm diameter and 40-mm length were deformed utilizing side pressing with different reductions of 15, 20, 25, and 30%. Afterward, the specimens were cut into 3-mm length samples, and the samples were annealed isothermally at 600 and 700 °C. In order to determine the recrystallized fraction, samples were first held at recrystallization temperature for different holding durations and rapidly cooled. For each sample, the hardness values were measured in ten regions along horizontal direction from the center to the surface of the specimens while the distance of each region from the center was determined based on the results of the deformation analysis. In the final stage, the recrystallized fraction in each region was calculated by the following relationship:

$$\%X = \frac{\text{HV}_d - \text{HV}_t}{\text{HV}_d - \text{HV}_a} \quad \text{(Eq 12)}$$

here HV_d is the hardness of the deformed material, HV_t the hardness of the annealed material at time t, and HV_a is the hardness of the fully annealed material. In addition, the metallographic examination was performed on the cross section of specimens after applying conventional polishing techniques and etched with 2% Nital and the mean grain size in each region was measured according to the ASTM E112.

Table 2 Chemical composition of the low carbon steel examined in this study (wt.%)

C	Mn	S, max	P, max	N, ppm
0.06	0.55	0.003	0.003	120

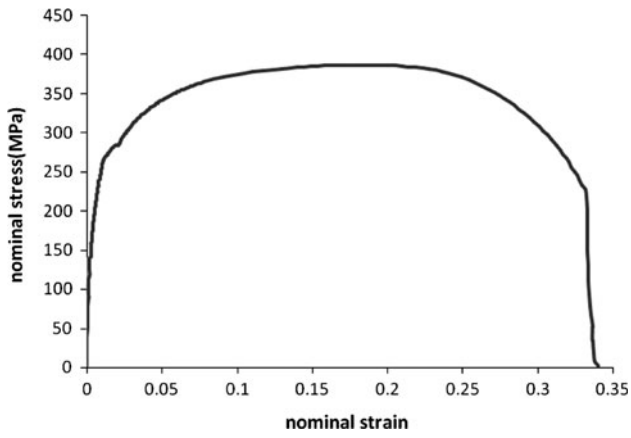

Fig. 2 Nominal stress-strain diagram of the steel used in this research

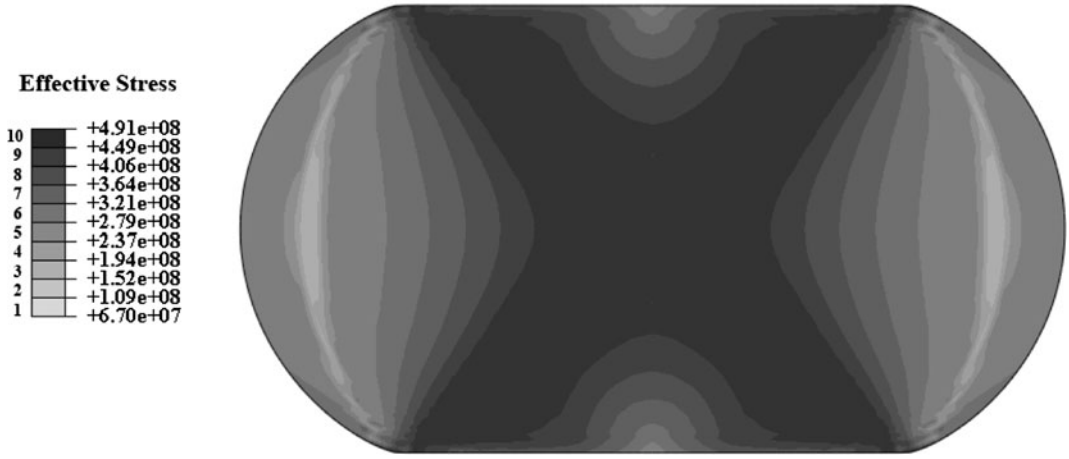

Fig. 3 Effective stress distribution of the side-pressed specimen for reduction of 25%

Table 3 Stored energy of deformation at different regions of the side-pressed specimens (MJ/m^3)

Reduction, %	1	2	3	4	5	6	7	8	9	10
15	0.48	0.74	1.05	1.4	1.82	2.25	2.81	3.37	4.00	4.52
20	0.56	0.86	1.24	1.68	2.18	2.74	3.39	4.08	4.84	5.34
25	0.65	0.97	1.37	1.82	2.36	2.94	3.61	4.33	5.13	5.76
30	0. 78	1.01	1.55	1.98	2.54	3.33	4.20	5.06	6.25	7.5

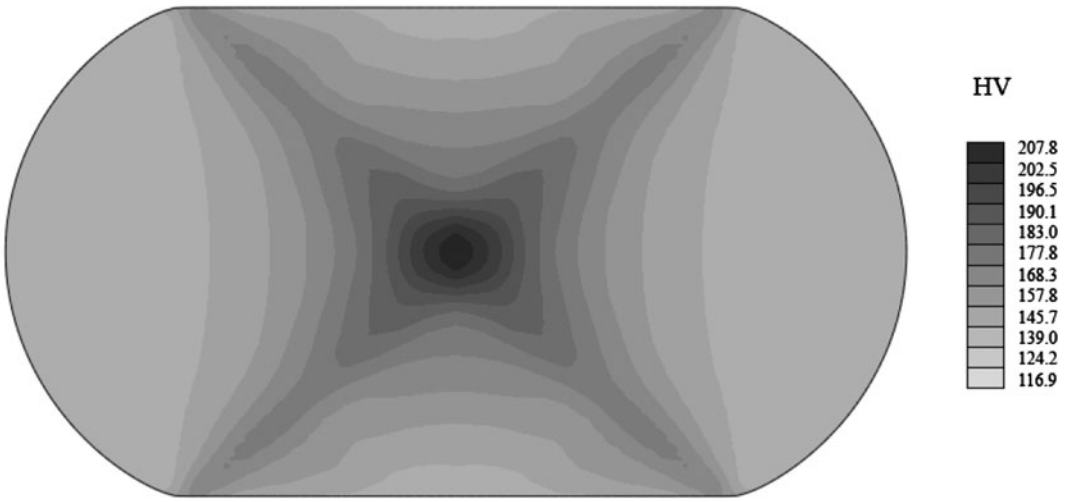

Fig. 4 Measured hardness distribution of the side-pressed specimen for reduction of 25%

4. Results and Discussion

The effective stress field achieved by the deformation analysis for side pressing operation is shown in Fig. 3. It is clear that the stress is distributed non-uniformly and even shear band-like regions are formed within the steel. While the maximum and minimum effective stresses and corresponding stored energy are achieved at the center and the edge of the specimen, respectively. Accordingly, the inhomogeneous deformation field leads to non-uniform distribution of stored energy as shown in Table 3. To examine the validity of FEA results, the hardness distribution which is achieved by Vickers hardness measurement is compared with the predicted stress distribution as shown in Fig. 3 and 4. It is observed that there is a reasonable agreement between the predictions and the experimental results.

In this study, regions with different amount of stored energy, namely, regions 1-10 were used in the recrystallization modeling. The calculated stored energies at different reductions are listed in Table 3. It is expected that as the effective stress increases from regions 1 to 10, the stored energy also increases. Furthermore, with increasing amount of reduction, the stored energy is expected to be increased as well. Figure 5 shows the nucleation steps in different regions within the deformed specimen for reduction of 25%. It is seen that in region having lower stored energy, nuclei are mostly formed on the grain

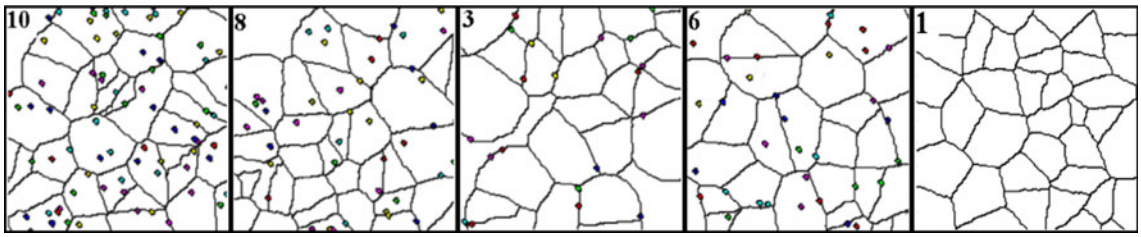

Fig. 5 Nucleation progress for different regions of the side-pressed specimen reduction of 25% at 600 °C

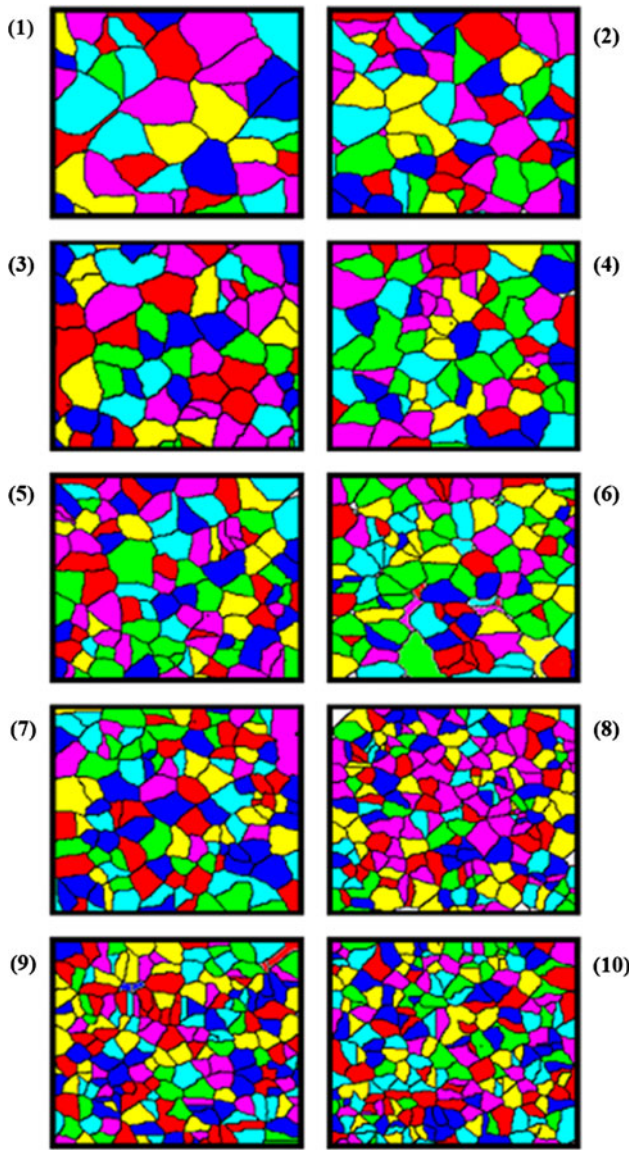

Fig. 6 Grain size distribution in different regions of the side-pressed specimen reduction of 15% at 600 °C

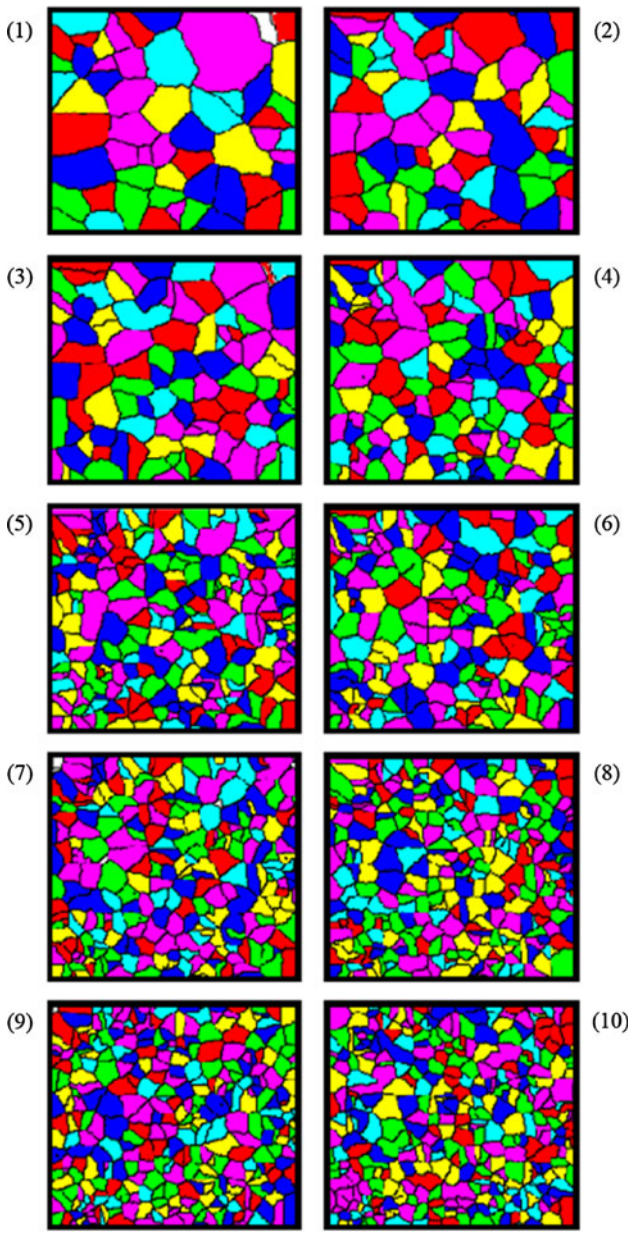

Fig. 7 Grain size distribution in different regions of the side-pressed specimen reduction of 30% at 600 °C

boundaries. However, with increasing stored energy owing to higher plastic deformations, stored energy within the grains is high enough to promote nucleation inside the grains as indicated in regions 8 and 10 in this figure. Figures 6 and 7 show the recrystallized microstructure of side-pressed specimen after reductions of 15 and 30% at 600 °C. It is observed that the minimum grain size is achieved in the center of the deformed sample. This is because more nucleation sites are formed within the region with higher internal stored energy (Ref 1). Comparing Fig. 6 and 7, it can be seen that the grain size of each region

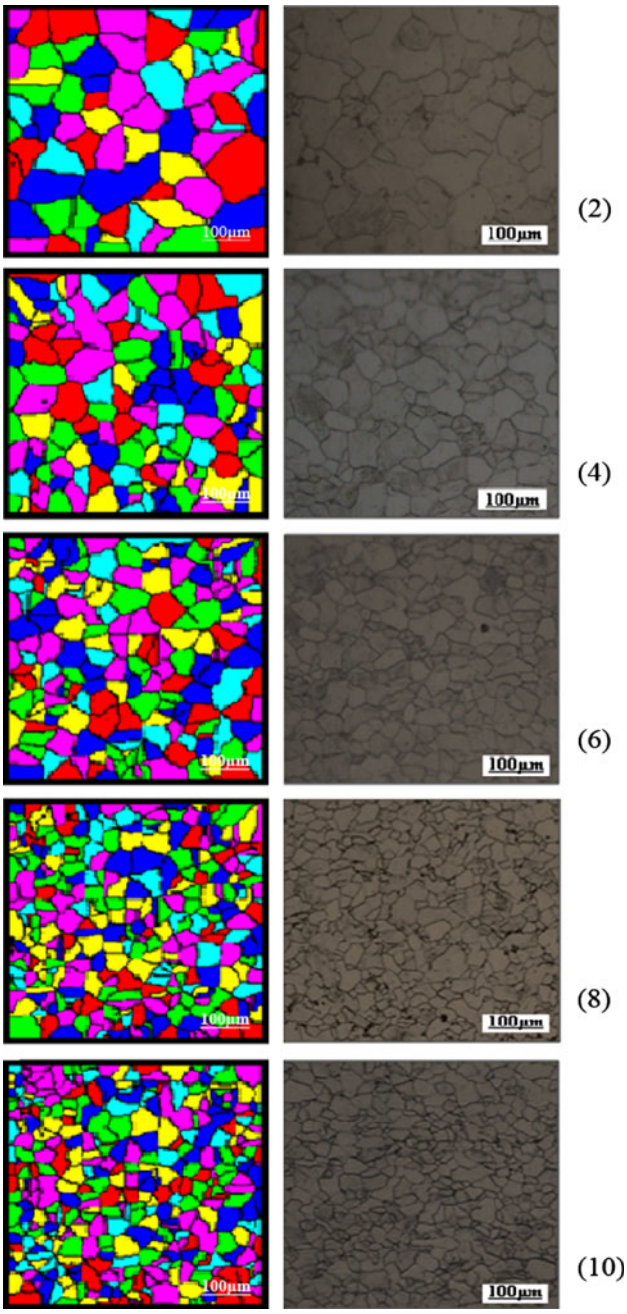

Fig. 8 Experimental and corresponding predicted results for grain size distribution in different regions after reduction of 30% at 600 °C

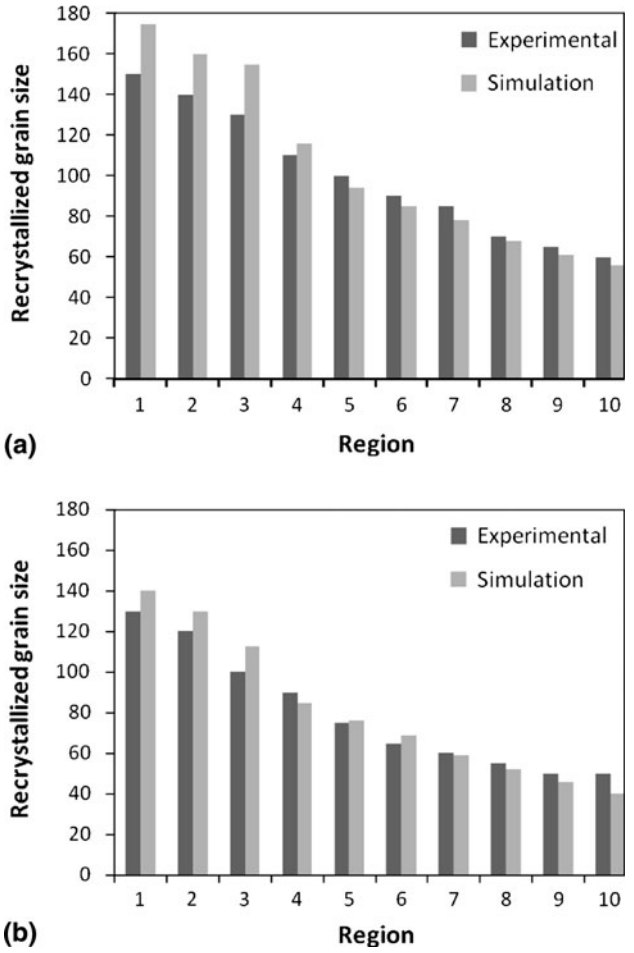

Fig. 9 Predicted and experimental results of recrystallized grain size in different regions after recrystallization at 600 °C: (a) reduction of 15% and (b) reduction of 25%

also decreases with increasing reduction as it is expected. The predicted recrystallized microstructures of the side-pressed specimen after 30% reduction and recrystallized at 600 °C is also compared with the metallographic results for the same conditions in Fig. 8. It can be seen that there is a reasonable agreement between the predicted and the real microstructures.

The metallographic observations were performed on the side-pressed and recrystallized samples, and the mean grain size for each region was also measured. The predicted grain size and the experimental mean grain size are compared for different regions under reductions of 15 and 30% at 600 °C, as shown in Fig. 9. The grain size of the model predictions is close to the experimental values while the average relative error of 9% is found in grain size prediction.

Using the stored energy calculated by FEA and CA model, the recrystallized fractions of the specimens under different reductions were also calculated as displayed in Fig. 10. These curves show the sigmoidal shape which agree with the well-known JMAK (Johnson-Mehl-Avrami-Kolmogrov) equation that can be expressed as (Ref 1):

$$X = 1 - \exp(-Bt^n) \quad \text{(Eq 13)}$$

here X is recrystallized fraction, t is time, and B and n are material constants. It is seen that with increasing reduction, recrystallization kinetics become faster due to higher stored energy, while the same experimental results have been reported by others (Ref 24, 25). In general, recrystallization kinetics can be evaluated by the time for 50% recrystallization ($t_{0.5}$). In Fig. 11, the simulated results for 50% recrystallization are compared with the experimental data which are calculated from the results of hardness testing. It is seen that there is a reasonable consistency between the calculated and the experimental ones where $t_{0.5}$ decreases by increasing amount of plastic deformation, which indicates faster static recrystallization kinetics. This result is in agreement with the other studies (Ref 26, 27) as well as modeling studies (Ref 11, 28-31).

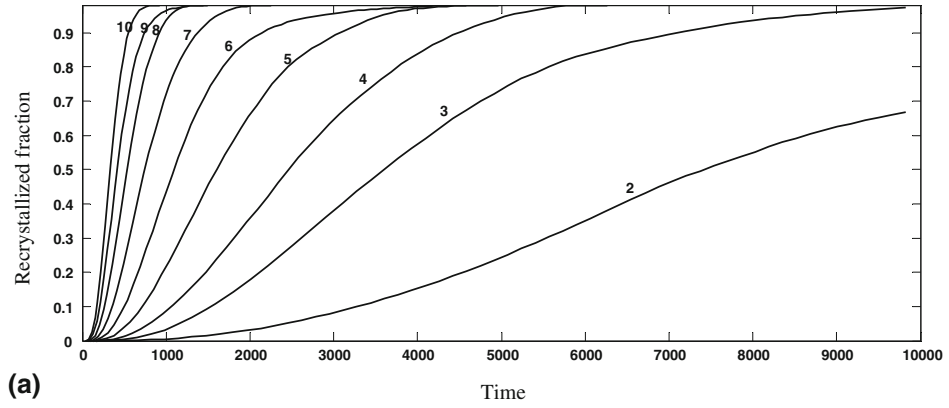

(a)

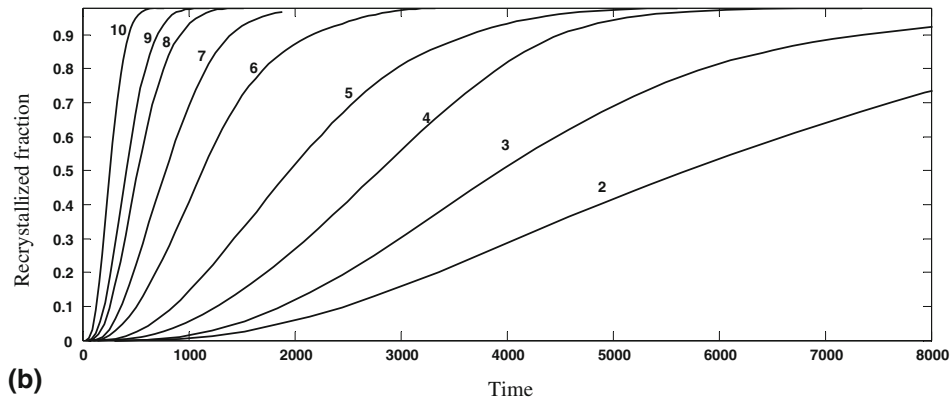

(b)

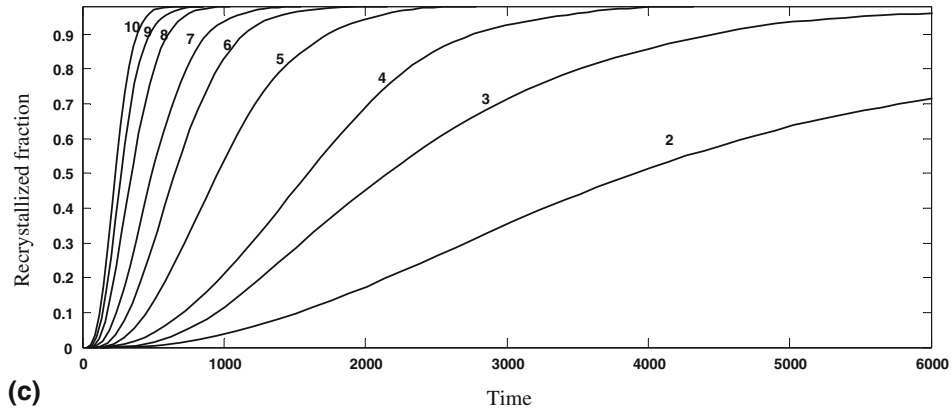

(c)

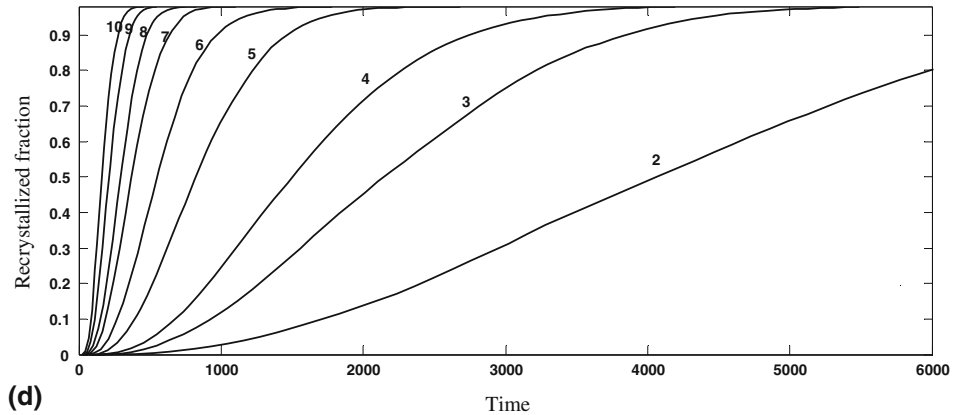

(d)

Fig. 10 The recrystallized fraction vs. time in different regions at 600 °C for reduction of (a) 15%, (b) 20%, (c) 25%, and (d) 30%

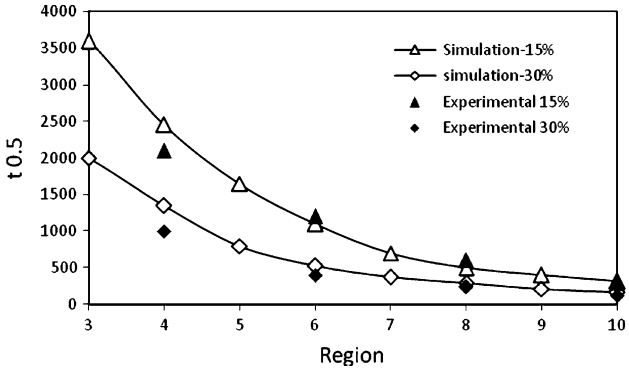

Fig. 11 Comparison between predicted and experimental $t_{0.5}$ in different reductions

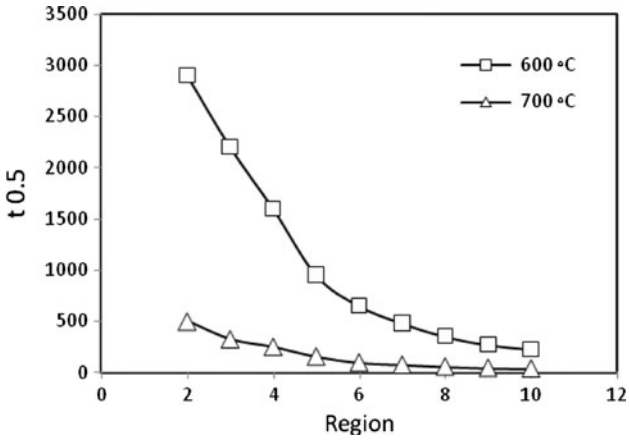

Fig. 12 Comparison between predicted and experimental $t_{0.5}$ values in different temperatures

Figure 12 compares the time for 50% recrystallization at 600 and 700 °C for the specimen with reduction of 25%. As it is expected, increasing the temperature causes higher diffusion rate as well as increases recrystallization front velocity, and thus, recrystallization kinetics accelerated at high temperatures. This result is in agreement with the experimental observations in many alloys (Ref 28). Therefore, it can be concluded that this simulation properly considers the effect of temperature on recrystallization kinetic.

It is interesting to mention that by increasing the stored energy in different regions, the required time for recrystallization completion decreases. In other words, recrystallization completion of inhomogeneously deformed specimen depends on the kinetic of recrystallization in the region with the lowest stored energy. Therefore, in each amount of reduction, the optimum time for completion of recrystallization can be calculated using the kinetic result of region with the lowest stored energy. This point can be particularly important for determination of an appropriate annealing time for large industrial parts.

5. Conclusion

The static recrystallization of inhomogeneously deformed low carbon steel has been investigated at different reductions by coupling the finite element analysis with a cellular automata model. The deformation analysis first provides the stored energy distribution within the cold deformed steel and then cellular automata model predicts the kinetics of subsequent recrystallization process. The side pressing of cylindrical samples has been studied by the model, and the following results have been achieved:

- The distribution of recrystallized grains is inhomogeneous in side-pressing experiments as a result of the heterogeneous distribution of the stored energy and the minimum grain size is achieved at the center of the specimen.
- At low strains, the nuclei mainly develop on the original grain boundaries; however, by increasing deformation, some nuclei also form within the grains.
- By comparing the modeling results and the experimental data, it is found that the presented model can reasonably predict the kinetics of recrystallization and recrystallized microstructures.

References

1. F.J. Humphreys and M. Hatherly, *Recrystallization and Related Annealing Phenomena*, Elsevier Science, Oxford, 2006
2. D. Hull and D.J. Bacon, *Introduction to Dislocations*, 3rd ed., Pergamon Press, Oxford, 1984
3. D. Raabe, F. Roters, F. Barlat, and L.Q. Chen, Ed., *Continuum Scale Simulation of Engineering Materials*, Willey-VCH, Weinheim, 1998
4. G.F. Janssens, D. Raabe, E. Kozeschnik, M.A. Miodownik, and B. Nestler, *Computational Materials Engineering*, Elsevier Academic Press, London, UK, 2007
5. H.W. Hesselbarth and I.R. Gobel, Simulation of Recrystallization by Cellular Automata, *Acta Metal. Mater.*, 1991, **39**, p 2135–2143
6. R.L. Goetz and V. Seetharaman, Static Recrystallization Kinetics with Homogeneous and Heterogeneous Nucleation Using a Cellular Automata Model, *Metall. Mater. Trans.*, 1998, **29A**, p 2307–2321
7. C.H.J. Davies, The Effect of Neighborhood on the Kinetics of a Cellular Automaton Recrystallization Model, *Scripta Metall. Mater.*, 1995, **33**, p 1139–1143
8. C.H.J. Davies, Growth of Nuclei in a Cellular Automaton Simulation of Recrystallization, *Scripta Metall. Mater.*, 1997, **36**, p 35–40
9. V. Marx, F.R. Reher, and G. Gottestin, Simulation of Primary Recrystallization Using a Modified Three-Dimensional Cellular Automation, *Acta Mater.*, 1999, **47**, p 1219–1230
10. D. Raabe and R. Becker, Coupling of a Crystal Plasticity Finite Element Model with a Probabilistic Cellular Automaton for Simulating Primary Static Recrystallization in Aluminum, *Modell. Simul. Mater. Sci. Eng.*, 2000, **8**, p 445–462
11. G. Kugler and R. Turk, Study of the Influence of Initial Microstructure Topology on the Kinetics of Static Recrystallization Using a Cellular Automata Model, *Comput. Mater. Sci.*, 2006, **37**, p 284–291
12. P.J. Hurley and F.J. Humphreys, Modeling the Recrystallization of Single-Phase Aluminum, *Acta Mater.*, 2003, **51**, p 3779–3793
13. R. Dewri and N. Chakraborti, Simulating Recrystallization Through Cellular Automata and Genetic Algorithms, *Modell. Simul. Mater. Sci. Eng.*, 2005, **13**, p 173–183
14. P.R. Rios and J.C. Pereira, Comparison of Analytical Models with Cellular Automata Simulation of Recrystallization in Two Dimensions, *Mater. Res.*, 2005, **8**, p 341–345
15. P.R. Rios and J.C. Pereira, Microstructural Descriptors and Cellular Automata Simulation of the Effects of Non-Random Nuclei Location on Recrystallization in Two Dimensions, *Mater. Res.*, 2006, **9**, p 165–170
16. G.F. Janssens, Random Grid, Three-Dimensional, Space-Time Coupled Cellular Automata for the Simulation of Recrystallization and Grain Growth, *Modell. Simul. Mater. Sci. Eng.*, 2003, **11**, p 157–171

17. R.L. Goetz and V. Seetharaman, Modeling Dynamic Recrystallization Using Cellular Automata, *Scripta Metall. Mater.*, 1998, **38**, p 405–413
18. R. Ding and Z.X. Guo, Coupled Quantitative Simulation of Microstructural Evolution and Plastic Flow During Dynamic Recrystallization, *Acta Mater.*, 2001, **49**, p 3163–3175
19. J. Kroc, Application of Cellular Automata Simulations to Modeling of Dynamic Recrystallization, *Comput. Sci.*, 2329, **2002**, p 773–782
20. M. Qian and Z.X. Guo, Cellular Automata Simulation of Microstructural Evolution During Dynamic Recrystallization of an HY-100 Steel, *Mater. Sci. Eng. A*, 2004, **365**, p 180–185
21. G. Kugler and R. Turk, Modeling the Dynamic Recrystallization Under Multi-Stage Hot Deformation, *Acta Mater.*, 2004, **52**, p 4659–4668
22. X. Song, M. Rettenmayr, C. Müller, and H.E. Exner, Modeling of Recrystallization After Inhomogeneous Deformation, *Metall. Mater. Trans.*, 2001, **32A**, p 2199–2206
23. N. Hansen and B. Ralph, The Strain and Grain Size Dependence of the Flow Stress of Copper, *Acta Mater.*, 1982, **30**, p 411–417
24. M. Oyarzabal, A. Martınez-de-Guerenu, and I. Gutierrez, Effect of Stored Energy and Recovery on the Overall Recrystallization Kinetics of a Cold Rolled Low Carbon Steel, *Mater. Sci. Eng. A*, 2008, **485**, p 200–209
25. D. Rollett, D.J. Srolovitz, R.D. Doherty, and M.P. Anderson, Computer Simulation of Recrystallization Non-Uniformly Deformed Metals, *Acta Mater.*, 1989, **37**, p 1248–1254
26. R. Mendoza, A. Molina, F. Serrania, and J.A. Juarez-Islas, Mechanical Properties of a Recrystallized Low Carbon Steel, *Scripta Mater.*, 2003, **48**, p 391–395
27. H.W. Luo, J. Sietsma, and S. van der Zwaag, Effect of Inhomogeneous Deformation on the Recrystallization Kinetics of Deformed Metals, *ISIJ Int.*, 2004, **44**, p 1931–1939
28. P.N. Kalu and D.R. Waryoba, A JMAK-Microhardness Model for Quantifying the Kinetics of Restoration Mechanisms in Inhomogeneous Microstructure, *Mater. Sci. Eng. A*, 2007, **464**, p 68–75
29. X. Song and M. Rettenmayer, Modeling Study on Recrystallization, Recovery and their Temperature Dependence in Inhomogeneously Deformed Materials, *Mater. Sci. Eng. A*, 2002, **332**, p 153–160
30. Y.C. Lin, M. Chen, and J. Zhong, Study of Static Recrystallization Kinetics in a Low Alloy Steel, *Comput. Mater. Sci.*, 2008, **44**, p 316–321
31. M. Kazeminezhad, On the Modeling of the Static Recrystallization Considering the Initial Grain Size Effects, *Mater. Sci. Eng. A*, 2008, **486**, p 202–207